A MEASUREMENT OF THE Z^0 INVISIBLE WIDTH BY SINGLE PHOTON COUNTING

Dean Karlen
Carleton University

Representing the OPAL collaboration

Abstract

The OPAL detector at LEP is used to measure the partial decay width of the Z^0 into invisible particles by measuring the cross section of single photon events in e^+e^- collisions at centre-of-mass energies near the Z^0 resonance. In a data sample of 5.3 pb^{-1}, we observe 73 events with single photons depositing more than 1.5 GeV in the electromagnetic calorimeter, with an expected background of 8 ± 2 events. With this data we determine the Z^0 invisible width to be $0.50 \pm 0.07 \pm 0.03$ GeV, where the first error is statistical and the second systematic. This corresponds to $3.0 \pm 0.4 \pm 0.2$ light neutrino generations in the Standard Model.

Introduction

Electron-positron collisions at centre-of-mass energies near and above the Z^0 resonance provide an opportunity to determine the content of light matter which interacts only through the weak force. Such particles contribute to the Z^0 invisible width, Γ_{inv}, if their masses are less than $M_{Z^0}/2$. In the Standard Model the invisible width is expected to be[1] 0.500 ± 0.005 GeV from the three neutrino species. Precision measurements of Γ_{inv} have been made so far by subtracting the observed widths into multihadrons and charged leptons from the total width.[2,3] Our most recent result[2] obtained this way is 0.509 ± 0.015 GeV. This method, however, assumes that all visible decays of the Z^0 are accounted for in the analyses of the charged leptons and multihadrons.

In this talk we describe a complementary analysis[4] that directly measures the invisible width by determining the cross section for events where the Z^0 decays into invisible particles. The events are signalled by a photon arising from initial state radiation. The cross section for the process $e^+e^- \rightarrow \nu\bar{\nu}\gamma$ is roughly proportional to the Z^0 invisible width, since it is dominated by the amplitude given by the Feynman diagram shown in figure 1a. The contribution from W exchange, shown in figure 1b, is less than 5 % for centre-of-mass energies between the Z^0 mass and 10 GeV above.[5]

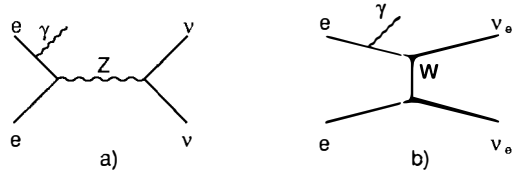

Figure 1. Two of the Feynman diagrams which contribute in lowest order to the process $e^+e^- \rightarrow \nu\bar{\nu}\gamma$. a) Z^0 decay allows the production of any of the light neutrino species. b) W exchange produces only electron neutrinos.

The OPAL detector

The OPAL detector is described in detail elsewhere.[6] Charged particle tracking is provided by the central detector, consisting of the vertex, jet, and z chambers. The central detector is contained inside a pressure vessel and a solenoidal coil; a total of 1.8 radiation lengths of material at normal incidence. The electromagnetic calorimeter consists of barrel and endcap arrays of lead glass blocks which cover the solid angle $|\cos\theta| < 0.98$. Just in front of the barrel lead glass blocks are time-of-flight (TOF) scintillation counters and gas presampler detectors. Figure 2 shows the orientation of these detector elements.

The return yoke of the magnet surrounds the lead glass arrays and is instrumented to form the hadron calorimeter. Barrel and endcap muon detectors complement the muon identification with four layers of chambers outside the hadron calorimeter.

The two forward detectors, each consisting of calorimeters, proportional tube chambers, drift chambers and scintillators, provide a luminosity measurement by counting low angle Bhabha events. In this analysis, the calorimeters are also used to veto events with an electron or a second photon scattering above 2°.

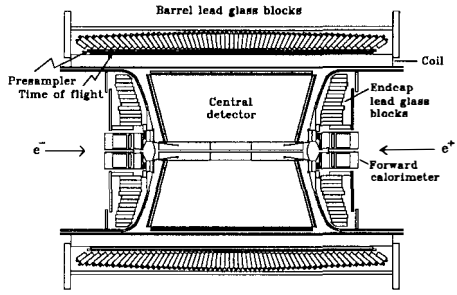

Figure 2. A cross section of the OPAL central detector and electromagnetic calorimetry.

Events with only a single photon in the barrel region are recorded if a barrel electromagnetic calorimeter cluster exists with energy above approximately 3 GeV, or with energy above approximately 1 GeV provided a nearby TOF counter fired within 40 ns of the beam crossing. Approximately 80 % of photons with normal incidence on the coil convert before reaching the TOF counters.

The threshold behaviour of these triggers is studied by using events with a single electron in the barrel region. Such events are also recorded if either a track is found by the trigger electronics that matches with an electromagnetic cluster above approximately 1 GeV, or a track is found with a nearby TOF counter.

Single electron analysis

To study the problems associated with the low energy single photon measurement, we use events with single electrons scattered at large angles as a high statistics control sample. Such events are selected by requiring that only one track exist and its momentum transverse to the beam axis be greater than 1 GeV. There must be an electromagnetic cluster with at least 500 MeV of energy deposited within $|\cos\theta| < 0.7$ and within 200 mrad of the track direction. The event must not contain a second cluster above 300 MeV in the barrel or endcap electromagnetic calorimeters. Single muon events are removed by requiring the mean energy loss as measured in the jet chamber, dE/dx, to be greater than 9 keV/cm, which is 98 % efficient for the single electron events.

A total of 5980 events satisfy these criteria. The observed transverse momentum and angular distributions of the events are shown in figure 3 to be described by the lowest order Monte Carlo expectations from radiative Bhabha scattering[7] $e^+e^- \rightarrow e^+e^-\gamma$ and two photon production[8] of electron pairs $e^+e^- \rightarrow e^+e^-e^+e^-$. The ratio of the observed cross section to that expected from these calculations is 0.96 ± 0.01 (stat) ± 0.02 (sys). Events satisfying the track-TOF trigger coincidence are used to determine the efficiency of the calorimeter triggers and the results are shown in figure 3c.

Single photon analysis

Single photon candidates are selected by requiring the following:

(1) A cluster must be present in the region $|\cos\theta| < 0.7$ with deposited energy greater

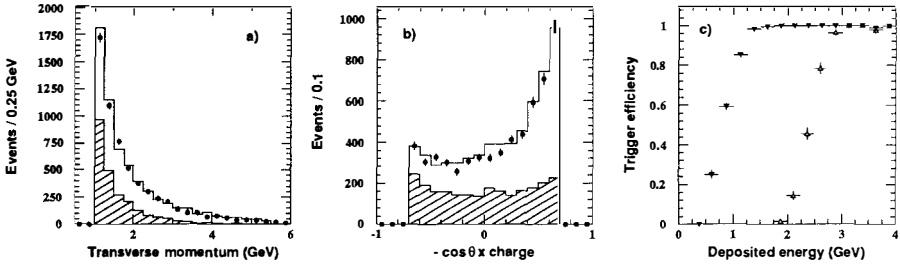

Figure 3. a) The observed transverse momentum spectrum and b) the angular distribution of single electron events compared with Monte Carlo expectations normalised to the integrated luminosity. The shaded histograms show the contribution from the reaction $e^+e^- \rightarrow e^+e^-e^+e^-$, while the unshaded areas show the part from $e^+e^- \rightarrow e^+e^-\gamma$. c) The efficiencies of the barrel electromagnetic calorimeter triggers as determined from these events. The solid triangles show the behaviour of the low threshold trigger which is used in coincidence with a track or TOF counter. The open triangles show the stand alone high threshold trigger.

than 1 GeV. The cluster is required to not extend more than 200 mrad in the polar or azimuthal directions, which removes cosmic ray and beam halo muons which graze the barrel lead glass block array.

(2) No other cluster may be present anywhere in the barrel or endcap electromagnetic calorimeters with more than 300 MeV deposited energy.

(3) There must be no reconstructed central detector track with 20 or more jet chamber hits.

(4) To remove background from beam wall and beam gas interactions, the event must contain no vertex (jet) chamber sector with 5 (50) or more hits.

(5) The energy deposited in each forward calorimeter must be less than 2 GeV.

(6) To remove background from cosmic ray and beam halo events, a match must exist between the calorimeter cluster and a presampler cluster.

(7) Remaining cosmic ray events are rejected if there are muon signals in the hadron calorimeters or muon chambers.

There is a total of 136 events which satisfy these criteria. Since backgrounds are smaller and better understood for higher energy single photons, only the 73 events with single photons depositing more than 1.5 GeV in the calorimeter are used to determine the Z^0 invisible width. The events between 1 and 1.5 GeV are used as a background control sample, with which to verify the background estimates.

The efficiency of the single photon selection, summarised in table 1, is determined from a variety of data samples. These include the single electron sample as described above, single photon events from the processes $e^+e^- \rightarrow e^+e^-\gamma$ and $e^+e^- \rightarrow \gamma\gamma\gamma$ which are tagged by energy in the forward calorimeters, $e^+e^- \rightarrow \gamma\gamma$ events, isolated photons from $e^+e^- \rightarrow l^+l^-\gamma$, where l is an electron or muon and both leptons are scattered at wide angles, and a sample of more than 80,000 random beam crossing events.

Various backgrounds to the $e^+e^- \rightarrow \nu\bar{\nu}\gamma$ process coming from electron positron interactions are estimated from Monte Carlo calculations and summarised in table 1. The dominant background comes from low Q^2 radiative Bhabha scattering, in which both electrons escape detection at small angles with respect to the beam axis.

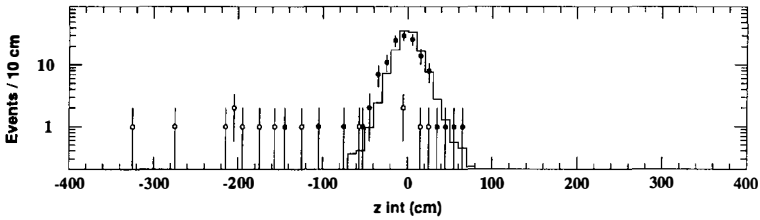

Figure 4. The estimate, $z_{\rm int}$, of the z coordinate of the interaction producing the photon, using the time of arrival at the TOF counters. Upstream production corresponds to $z_{\rm int} < 0$, which is expected for beam wall or beam gas production. The histogram is the distribution of the single electron sample, normalised to the single photon sample. The single photon candidates are indicated by the solid points. The open circles show beam gas - beam wall candidate events; those which fail the selection only by requirement (4).

No background from cosmic ray and beam halo muons is observed; the time-of-flight measurements from the single photon candidates are all found to be within 2 ns of the expected flight time.

Background events resulting from an interaction of a beam electron with the gas inside the LEP ring or with the beam pipe wall can generate photons from any point along the beam axis. Such events will tend to originate from a interaction upstream of the nominal collision point, and hence the particles will arrive at a TOF counter earlier than expected for a photon coming from an interaction at the origin. The measured time after the beam crossing is thus used to estimate the z coordinate of the interaction which produced the photon, $z_{\rm int}$, as shown in figure 4. Assuming a uniform population along the beam axis for beam wall and beam gas events which satisfy the single photon selection, we estimate the contamination of such events in the sample of single photons above 1 GeV to be 2 ± 2 events.

For a precise measurement of the single photon cross section, at centre-of-mass energies near the Z^0 mass, it is essential to understand the scale of the photon energy measurement, since the photon spectrum is a rapidly falling distribution. The single electron sample is used to study the simulation of energy loss in the coil, and the energy scale and resolution of the calorimeter. This study shows that the detector simulation of the photon energy measurement can be used directly. The energy scale uncertainty at 1.5 GeV is assumed to be 30 MeV, which corresponds to an uncertainty in the single photon acceptance of 2.1 % for the single photon sample above 1.5 GeV.

Results

A total of 73 single photon candidates depositing more than 1.5 GeV in the calorimeter is observed in the data sample of 5.3 $\rm pb^{-1}$ used in this analysis. Table 2 shows the luminosity and the number of single photon candidates recorded at each of the seven centre-of-mass energy points. The single photon spectra of deposited energies at each of the centre-of-mass energies are shown in figure 5 along with the Monte Carlo expectations for the process[9] $e^+e^- \rightarrow \nu\bar{\nu}\gamma$, assuming three generations of light neutrinos, and with the backgrounds from the sources discussed above. The angular distributions are shown in figure 6 for deposited energies below and above 1.5 GeV. In general, good agreement is observed.

Table 1. Summary of the efficiency of the single photon selection and the background estimates, separated for the samples below and above 1.5 GeV in deposited energy. The occupancy vetos refer to the occupancy requirements in the electromagnetic calorimeter, the vertex and jet chambers, the forward calorimeters, and the hadron calorimeter and muon detectors, from criteria (2), (4), (5), and (7). The backgrounds are quoted as the number of events expected to contribute to the observed single photon sample.

	$1 < E < 1.5$ GeV	$E > 1.5$ GeV
Efficiencies (%)		
trigger	89.2 ± 3.1	98.7 ± 0.1
occupancy vetos	97.5 ± 0.1	97.5 ± 0.1
no conversion in central detector	94 ± 2	94 ± 2
conversion in coil	82 ± 3	82 ± 3
presampler match	97 ± 2	97 ± 2
total efficiency (%)	65.0 ± 3.8	72.0 ± 3.4
Backgrounds (events)		
$e^+e^- \to e^+e^-\gamma$	13 ± 2	5 ± 1
$e^+e^- \to \gamma\gamma\gamma$	1 ± 1	–
$e^+e^- \to e^+e^-X \ \ (X = f_2, \pi^0, \eta, \eta')$	6 ± 2	1 ± 1
$e^+e^- \to e^+e^-l^+l^-\gamma$	4 ± 4	–
$e^+e^- \to \mu^+\mu^-\gamma$	1 ± 1	1 ± 1
beam gas and beam wall interactions	1 ± 1	1 ± 1
total background (events)	26 ± 5	8 ± 2

Table 2. The luminosity and the number of single photon candidates which deposit between 1.0 and 1.5 GeV and more than 1.5 GeV in the calorimeter at each centre-of-mass energy point. The corrected cross sections, σ, are listed for single photon production for photons above 1.5 GeV in the angular region $|\cos\theta| < 0.7$ and with no restrictions against additional photons. The errors indicate the uncorrelated uncertainties only. In addition, there are correlated uncertainties of 5.6 % and 0.8 pb.

$E_{\rm cm}$ (GeV)	$\mathcal{L}$ (pb^{-1})	$E < 1.5$ GeV	$E > 1.5$ GeV	σ (pb)
88.22	0.400	5	2	6 ± 6
89.22	0.546	3	2	4 ± 4
90.22	0.264	2	2	10 ± 9
91.22	2.752	26	20	12 ± 4
92.22	0.379	5	5	21 ± 11
93.22	0.498	11	17	56 ± 14
94.22	0.473	11	25	87 ± 18

The corrected cross sections are shown in table 2 for the process $e^+e^- \to \nu\bar{\nu}\gamma$, where a photon is above 1.5 GeV in the angular region $|\cos\theta| < 0.7$ and with no restrictions placed against additional photons. These are determined by using the number of observed events and the integrated luminosity also shown in table 2, applying the efficiency and background corrections given in table 1, and then scaling the results by coefficients determined from the detector simulation to account for the energy loss. Finally, a correction of $+2 \pm 1$ % is applied to account for the restriction against a second photon depositing more than 300 MeV in the electromagnetic calorimeter. The overall systematic error from the uncertainties in these corrections and in the integrated luminosity is 5.6 %. In addition, there is an uncertainty in the corrected cross sections of 0.8 pb from the uncertainty of the background.

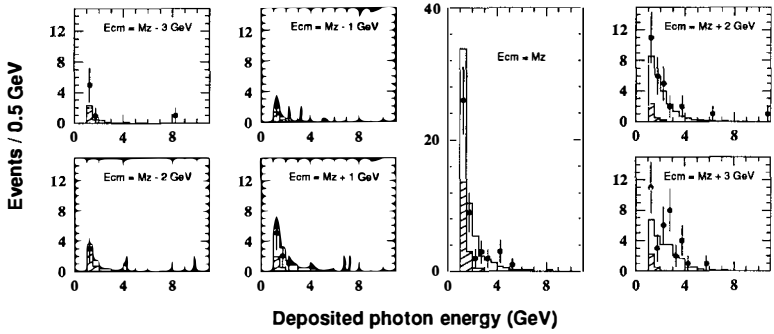

Figure 5. The energies deposited in the electromagnetic calorimeter by all the single photon candidates are shown at each of the seven centre-of-mass energy points. Also shown are Monte Carlo expectations, normalised to the recorded luminosities and corrected for trigger and selection efficiencies. The unshaded region of the histogram shows the prediction for the process $e^+e^- \to \nu\bar{\nu}\gamma$ assuming three generations of light neutrinos while the shaded portion corresponds to the component from background.

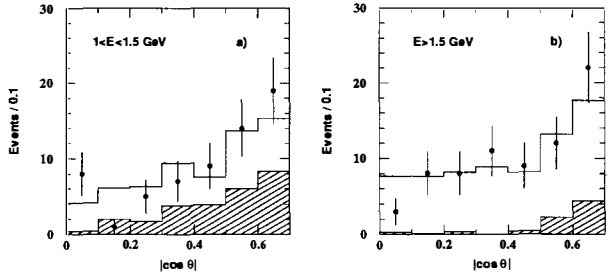

Figure 6. The angular distribution for the single photon candidates depositing a) between 1 and 1.5 GeV, b) more than 1.5 GeV in the electromagnetic calorimeter, from the complete data set. Also shown are Monte Carlo expectations, corrected for trigger and selection efficiencies, for the process $e^+e^- \to \nu\bar{\nu}\gamma$, assuming three generations of light neutrinos (unshaded areas), and the background sources (shaded histograms).

An analytical program[10,5] which evaluates the cross section for $e^+e^- \to \nu\bar{\nu}\gamma$ is used to determine the Z^0 invisible width. Here we assume that the W contribution is indeed given by the Standard Model, and that no other diagrams, other than those shown in figure 1, lead to final states with a single photon and no other visible particles. This analysis gives a Z^0 invisible width of $0.50 \pm 0.07 \pm 0.03$ GeV. Assuming the Standard Model Z^0 coupling to neutrinos, this corresponds to $3.0 \pm 0.4 \pm 0.2$ light neutrino generations. The corrected cross section is shown as a function of centre-of-mass energy in figure 7, along with the expectations for $N_\nu = 2, 3, 4$.

With this measurement of the invisible width, the number of single photon candidates which deposit between 1 and 1.5 GeV in the electromagnetic calorimeter is expected to be 64 ± 6 including backgrounds, in good agreement with the 63 observed events. By using these lowest energy events as a background control sample, the statistical significance of the complete single photon sample is reduced. However, this control sample provides an

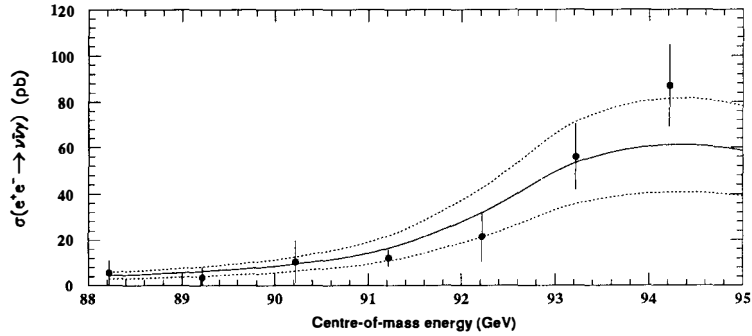

Figure 7. The corrected cross sections (pb) at each centre-of-mass energy point for single photons above 1.5 GeV in the angular range $|\cos\theta| < 0.7$ from the process $e^+e^- \to \nu\bar{\nu}\gamma$. The solid curve shows the result corresponding to 3.0 light neutrino generations. The expectations from two and four light neutrino generations are shown by the lower and upper dashed curves respectively.

important check of the background calculations using the data themselves.

It is a pleasure to thank the organisers of the 26$^{\text{th}}$ Rencontres de Moriond on Electroweak Interactions for a very enjoyable meeting in a stimulating environment.

REFERENCES

1. D. Yu. Bardin *et al.*, Berlin-Zeuthen preprint PHE 89-19. 1989.
2. OPAL collaboration, G. Alexander *et al.*, CERN-PPE/91-67, April 1991.
3. G. J. Bobbink, *Status of Z^0 lineshape measurements at LEP*, these proceedings;
   ALEPH collaboration, D. Decamp *et al.*, Zeit. Phys. C48 (1990) 365;
   DELPHI collaboration, P. Abreu *et al.*, contribution to 25th International Conference on High Energy Physics, Singapore, CERN-PPE/90-119, August 1990;
   L3 collaboration, B. Adeva *et al.*, L3 preprint 029, February 1991.
4. OPAL collaboration, M. Z. Akrawy *et al.*, CERN-PPE/90-187, December 1990.
5. L. Trentadue *et al.* in *Z Physics at LEP1*, G. Altarelli ed., CERN 89-08 (1989) 129.
6. OPAL collaboration, K. Ahmet *et al.*, submitted to Nucl. Instr. and Meth., CERN-PPE/90-114, August 1990.
7. D. Karlen, Nucl. Phys. B289 (1987) 23.
8. R. Battacharya, J. Smith and G. Grammer, Phys. Rev. D15 (1977) 3267;
   J. Smith, J. A. M. Vermaseren and G. Grammer, Phys. Rev. D15 (1977) 3280.
9. R. Miquel, C. Mana and M. Martinez, Zeit. Phys. C48 (1990) 309;
   F. A. Berends, G. Burgers, C. Mana, M. Martinez and W. L. van Neerven, Nucl. Phys. B301 (1988) 583.
10. O. Nicrosini and L. Trentadue, Nucl. Phys. B318 (1989) 1.